Journal of Sound and Vibration (1997) **201**(1), 1–22

MOVING FORCE IDENTIFICATION: A TIME DOMAIN METHOD

S. S. Law and T. H. T. Chan

Department of Civil and Structural Engineering, Hong Kong Polytechnic University, Hunghom, Kowloon, Hong Kong

AND

Q. H. Zeng

Institute of Vibration Engineering, Nanjing University of Aeronautics and Astronautics, Nanjing 210016, *People's Republic of China*

(*Received* 10 *July* 1995, *and in final form* 12 *August* 1996)

The solution for the vertical dynamic interaction forces between a moving vehicle and the bridge deck is analytically derived and experimentally verified. The deck is modelled as a simply supported beam with viscous damping, and the vehicle/bridge interaction force is modelled as one-point or two-point loads with fixed axle spacing, moving at constant speed. The method is based on modal superposition and is developed to identify the forces in the time domain. Both cases of one-point and two-point forces moving on a simply supported beam are simulated. Results of laboratory tests on the identification of the vehicle/bridge interaction forces are presented. Computation simulations and laboratory tests show that the method is effective, and acceptable results can be obtained by combining the use of bending moment and acceleration measurements.

1. INTRODUCTION

An important type of inverse problem in structural mechanics is force identification or force reconstruction from measured structural responses. One major class of this problem is where the initiation site is known. Examples include determining the impact of aircraft on landing [1] and, in a more interesting case, the force on fruit [2]. Stevens [3] gives an excellent survey of the literature on the force identification problem as well as an overview of the subject. Another major class of problem is where both the force history and its location are unknown. Examples include using the modal response data to determine the location of impact forces on the read/write head of computer disks [4] and using wave propagation responses to determine the location of structural impacts [5].

The third class of problem is on the identification of moving forces on structure. Examples include vehicle/bridge interaction forces, which are important for bridge engineering. The forces are dependent on the bridge design parameters, the vehicle dynamics properties, the profile of the bridge surface and the speed of the moving vehicles. It is difficult to calculate the forces accurately, although a number of methods and models have been proposed. Since the forces are moving, it is difficult to measure them directly. These prompt the need for a technique to measure indirectly the moving forces from measurements of the response of the structure.

If the supporting beam model is taken as linear, the equations of motion of the beam model are often decoupled by modelling in the modal co-ordinates. Tunna [6] used the

0022–460X/97/110001 + 22 $25.00/0/sv960774

modal superposition technique to calculate wheel/rail contact forces due to wheel irregularities. The calculation of the modal parameters demands a linear track model and, if the damping distribution of the track is general, complex modal synthesis is adopted [7] to study the wheel/track interaction. O'Connor and Chan [8] used a convertible central difference to obtain speeds and accelerations from deflections or bending moments, and all response data are then substituted into the set of equations formed for the finite elements, to calculate the force directly.

In this paper an attempt is made to explore the theory of moving force identification. On the basis of the modal superposition principle, and assuming the force as a step function in a small time interval, a method is developed to identify the force in the time domain. The simulation of both one and two forces moving on a simply supported beam is used to evaluate the method. An experiment with a model car moving on a simply supported beam is performed to simulate the vehicle/bridge interaction problem, and the interaction forces are identified from measurements of bending moments and/or accelerations of the beam. Both the simulations and the experimental results show that the method is effective, and acceptable results can be obtained by combining the use of data from bending moment and acceleration measurements. The proposed method is noise sensitive, especially in identifying more than one moving force.

2. THEORY OF MOVING FORCE IDENTIFICATION

2.1. EQUATION OF MOTION AND MODAL SUPERPOSITION

The time varying force moving on a simply supported beam, as shown in Figure 1, is used to demonstrate the method. The beam is assumed to be of constant cross-section with constant mass per unit length, having linear, viscous proportional damping with small deflections, and the effects of shear deformation and rotary inertia (Bernoulli–Euler beam) are not taken into account. The force moves from left to right at a constant speed c. The equation of motion can be written as

$$\rho \frac{\partial^2 v(x,t)}{\partial t^2} + C \frac{\partial v(x,t)}{\partial t} + EI \frac{\partial^4 v(x,t)}{\partial x^4} = \delta(x - ct) f(t), \tag{1}$$

where $v(x, t)$ is the beam deflection at point x and time t, ρ is the mass per unit length, C is the viscous damping parameter, E is the Young's modulus of the material, I is the second moment of inertia of the beam cross-section, l is the length of the beam, $f(t)$ is the time varying point force, c is the speed of the force motion, and $\delta(t)$ is the Dirac delta function.

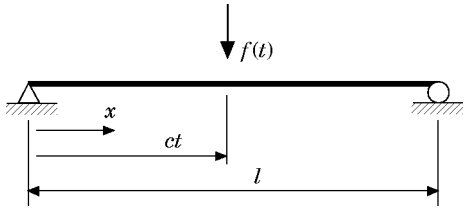

Figure 1. A simply supported beam subjected to a moving force $f(t)$.

Based on modal superposition, the dynamic deflection $v(x, t)$ can be described as follows:

$$v(x, t) = \sum_{n=1}^{\infty} \Phi_n(x) q_n(t), \tag{2}$$

where n is the mode number, $\Phi_n(x)$ is the mode shape function of the nth mode, and the $q_n(t)$ are the nth modal amplitudes. Substituting equation (2) into equation (1), and multiplying by $\Phi_j(x)$, integrating with respect to x between 0 and l, and applying the orthogonality conditions, we obtain

$$\frac{\mathrm{d}^2 q_n(t)}{\mathrm{d}t^2} + 2\xi_n \omega_n \frac{\mathrm{d}q_n(t)}{\mathrm{d}t} + \omega_n^2 q_n(t) = \frac{1}{M_n} p_n(t), \tag{3}$$

where ω_n is the modal frequency of the nth mode, ξ_n is the damping ratio of the nth mode, M_n is the modal mass of the nth mode, and $p_n(t)$ is the modal force. Based on assumptions for the beam, the modal parameters of the beam can be calculated as follows:

$$\omega_n = (n^2\pi^2/l^2)\sqrt{EI/\rho}\,, \qquad \Phi_n(x) = \sin(n\pi x/l), \tag{4, 5}$$

$$M_n = \rho l/2, \qquad p_n(t) = f(t) \sin(n\pi c t/l). \tag{6, 7}$$

For practical structures, the modal parameters can be obtained from the finite element model and/or modal testing.

Equation (3) can be solved in the time domain by the convolution integral, and yields

$$q_n(t) = \frac{1}{M_n} \int_0^t h_n(t - \tau) p(\tau) \mathrm{d}\tau, \tag{8}$$

where

$$h_n(t) = (1/\omega_n') \, \mathrm{e}^{-\xi_n \omega_n t} \sin(\omega_n' t), \quad t \geqslant 0, \qquad \omega_n' = \omega_n \sqrt{1 - \xi_n^2}. \tag{9, 10}$$

Substituting equations (8) and (5) into equation (2), the dynamic deflection of the beam at point x and time t can be found, as

$$v(x, t) = \sum_{n=1}^{\infty} \frac{2}{\rho l \omega_n'} \sin\frac{n\pi x}{l} \int_0^t \mathrm{e}^{-\xi_n \omega_n (t-\tau)} \sin\omega_n'(t - \tau) \sin\frac{n\pi c\tau}{l} f(\tau) \, \mathrm{d}\tau. \tag{11}$$

2.2. FORCE IDENTIFICATION FROM BENDING MOMENTS

The bending moment of the beam at point x and time t is

$$m(x, t) = -EI \frac{\partial^2 v(x, t)}{\partial x^2}. \tag{12}$$

Substituting equation (11) into equation (12) gives

$$m(x, t) = \sum_{n=1}^{\infty} \frac{2EI\pi^2 n^2}{\rho l^3 \omega_n'} \sin\frac{n\pi x}{l} \int_0^t \mathrm{e}^{-\xi_n \omega_n (t-\tau)} \sin\omega_n'(t - \tau) \sin\frac{n\pi c\tau}{l} f(\tau) \, \mathrm{d}\tau. \tag{13}$$

Assuming that the force $f(t)$ is a step function in a small time interval, equation (13) can be rewritten in discrete terms as

$$m(i) = \frac{2EI\pi^2}{\rho l^3} \sum_{n=1}^{\infty} \frac{n^2}{\omega_n'} \sin \frac{n\pi x}{l} \sum_{j=0}^{i} \mathrm{e}^{-\xi_n \omega_n \Delta t(i-j)} \sin \omega_n' \, \Delta t(i-j) \sin \frac{n\pi c \Delta t j}{l} f(j) \, \Delta t,$$

$$i = 0, 1, 2, \ldots, N, \tag{14}$$

where Δt is the sampling interval and $N+1$ is the number of sample points. Let

$$C_{xn} = \frac{2EI\pi^2}{\rho l^3} \frac{n^2}{\omega_n'} \sin \frac{n\pi x}{l} \Delta t, \tag{15}$$

$$E_n^k = \mathrm{e}^{-\xi_n \omega_n \Delta t k}, \qquad S_1(k) = \sin(\omega_n' \, \Delta t k), \qquad S_2(k) = \sin(n\pi c \Delta t k / l). \tag{16}$$

Arranging equation (14) into matrix form,

$$\begin{Bmatrix} m(0) \\ m(1) \\ m(2) \\ \vdots \\ m(N) \end{Bmatrix} = \sum_{n=1}^{\infty} C_{xn}$$

$$\times \begin{bmatrix} 0 & 0 & 0 & \cdots & 0 \\ 0 & 0 & 0 & \cdots & 0 \\ 0 & E_n^1 S_1(1) S_2(1) & 0 & \cdots & 0 \\ \vdots & \vdots & \vdots & \cdots & \vdots \\ 0 & E_n^{N-1} S_1(N-1) S_2(1) & E_n^{N-2} S_1(N-2) S_2(2) & \cdots & E_n^{N-N_B} S_1(N-N_B) S_2(N_B) \end{bmatrix}$$

$$\times \begin{Bmatrix} f(0) \\ f(1) \\ f(2) \\ \vdots \\ f(N_B) \end{Bmatrix}, \tag{17}$$

where

$$N_B = l / c \Delta t.$$

Assuming that

$$f(0) = 0, \qquad f(N_B) = 0 \tag{18}$$

at the entry and exit of a vehicle, we have, from equation (17),

$$m(0) = 0, \qquad m(1) = 0. \tag{19}$$

Equation (17) can then be condensed as

$$\begin{Bmatrix} m(2) \\ m(3) \\ \vdots \\ m(N) \end{Bmatrix} = \sum_{n=1}^{\infty} C_{xn} \begin{bmatrix} E_n^1 S_1(1)S_2(1) & 0 & \cdots & 0 \\ E_n^2 S_1(2)S_2(1) & E_n^1 S_1(1)S_2(2) & \cdots & 0 \\ \vdots & \vdots & \vdots & \vdots \\ E_n^{N-1} S_1(N-1)S_2(1) & E_n^{N-2} S_1(N-2)S_2(2) & \cdots & b_{ee} \end{bmatrix} \times \begin{Bmatrix} f(1) \\ f(2) \\ \vdots \\ f(N_B-1) \end{Bmatrix}, \tag{20}$$

where

$$b_{ee} = E_n^{N-N_B+1} S_1(N-N_B+1)S_2(N_B-1).$$

Equation (20) is simply rewritten as

$$\underset{(N-1)\times(N_B-1)}{\mathbf{B}} \quad \underset{(N_B+1)\times 1}{\mathbf{f}} = \underset{(N-1)\times 1}{\mathbf{m}} \tag{21}$$

If $N = N_B$, matrix $\mathbf{B}$ is a lower triangular matrix. We can find the force vector $\mathbf{f}$ directly by solving equation (21). If $N > N_B$ and/or N_l bending moments ($N_l > 1$) are measured, the least squares method can be used to find the force vector $\mathbf{f}$, from

$$\begin{bmatrix} \mathbf{B}_1 \\ \mathbf{B}_2 \\ \vdots \\ \mathbf{B}_{N_l} \end{bmatrix} \mathbf{f} = \begin{bmatrix} \mathbf{m}_1 \\ \mathbf{m}_2 \\ \vdots \\ \mathbf{m}_{N_l} \end{bmatrix}. \tag{22}$$

The above procedure is derived for single force identification. Equation (21) can be modified for two-forces identification using the linear superposition principle, as

$$\begin{bmatrix} \mathbf{B}_a & \mathbf{0} \\ \mathbf{B}_b & \mathbf{B}_a \\ \mathbf{B}_c & \mathbf{B}_b \end{bmatrix} \begin{Bmatrix} \mathbf{f}_1 \\ \mathbf{f}_2 \end{Bmatrix} = \mathbf{m}, \tag{23}$$

where $\mathbf{B}_a[N_s \times (N_B - 1)]$, $\mathbf{B}_b[(N - 1 - 2N_s) \times (N_B - 1)]$ and $\mathbf{B}_c[N_s \times (N_B - 1)]$ are sub-matrices of matrix $\mathbf{B}$. The first row of sub-matrices in the first matrix describes the state having the first force on the beam after its entry. The second and third rows of sub-matrices describe the states having two forces on the beam and one force on the beam after the exit of the first force. The whole matrix has a dimension of $(N - 1) \times (N_B - 1)$. $N_s = l_s/c\Delta t$, where l_s is the distance between two forces. The two forces can be identified using more than one measured bending moment measurement.

2.3. IDENTIFICATION FROM ACCELERATIONS

The acceleration at point x and time t is

$$\ddot{v}(x, t) = \sum_{n=1}^{\infty} \frac{1}{M_n} \Phi_n(x) \left[p_n(t) + \int_0^t \ddot{h}_n(t-\tau) p_n(\tau)\, \mathrm{d}\tau \right], \tag{24}$$

where

$$\ddot{h}_n(t) = \frac{1}{\omega_n'} \mathrm{e}^{-\xi_n \omega_n t} \{[\xi_n \omega_n)^2 - \omega_n'^2] \sin \omega_n' t + [-2\xi_n \omega_n \omega_n'] \cos \omega_n' t\}. \tag{25}$$

Equation (24) can be rewritten in discrete terms as

$$\ddot{v}(i) = \frac{2}{\rho l} \sum_{n=1}^{\infty} \sin \frac{n\pi x}{l} \left[\sin \frac{n\pi c \Delta t i}{l} f(i) + \sum_{j=0}^{i} \ddot{h}(i-j) \sin \frac{n\pi c \Delta t j}{l} f(j) \Delta t \right]. \tag{26}$$

The response of mode n is

$$\ddot{v}(i)_n = \frac{2}{\rho l} \sin \frac{n\pi x}{l} \left[\sin \frac{n\pi c \Delta t i}{l} f(i) + \frac{1}{\omega_n'} \sum_{j=0}^{i} \ddot{h}(i-j) \sin \frac{n\pi c \Delta t j}{l} f(j)\, \Delta t \right]. \tag{27}$$

Let

$$D_{xn} = \frac{2}{\rho l} \sin \frac{n\pi x}{l}, \qquad H_n(k) = \frac{\Delta t}{\omega_n'} \ddot{h}(k), \qquad S_2(k) = \sin\left(\frac{n\pi c \Delta t}{l} k\right). \tag{29}$$

Arranging equation (27) into matrix form,

$$\begin{Bmatrix} \ddot{v}(0) \\ \ddot{v}(1) \\ \ddot{v}(2) \\ \vdots \\ \ddot{v}(N) \end{Bmatrix}_n$$

$$= D_{xn} \begin{bmatrix} 0 & 0 & 0 & \cdots & 0 \\ 0 & S_2(1)(1 + H_n(0)) & 0 & \cdots & 0 \\ 0 & H_n(1) S_2(1) & S_2(2)(1 + H_n(0)) & \cdots & 0 \\ \vdots & \vdots & \vdots & \cdots & \vdots \\ 0 & H_n(N-1) S_2(1) & H_n(N-2) S_2(2) & \cdots & H_n(N - N_B) S_2(N_B) \end{bmatrix} \begin{Bmatrix} f(0) \\ f(1) \\ f(2) \\ \vdots \\ f(N_B) \end{Bmatrix} \tag{30}$$

Assuming that

$$f(0) = 0, \qquad f(N_B) = 0, \tag{31}$$

we have

$$\ddot{v}(0) = 0. \tag{32}$$

Equation (30) can be condensed as

$$\begin{Bmatrix} \ddot{v}(1) \\ \ddot{v}(2) \\ \vdots \\ \ddot{v}(N) \end{Bmatrix}_n = D_{xn} \begin{bmatrix} (1+H_n(0))S_2(1) & 0 & \cdots & 0 \\ H_n(1)S_2(1) & (1+H_n(0))S_2(2) & \cdots & 0 \\ \vdots & \vdots & \vdots & \vdots \\ H_n(N-1)S_2(1) & H_n(N-2)S_2(2) & \cdots & H_n(N-N_B+1)S_2(N_B-1) \end{bmatrix} \times \begin{Bmatrix} f(1) \\ f(2) \\ \vdots \\ f(N_B-1) \end{Bmatrix}. \quad (33)$$

Equation (33) is simply rewritten as

$$\underset{N\times 1}{\ddot{\mathbf{v}}_n} = \underset{N\times(N_B-1)}{\mathbf{A}_n} \underset{(N_B-1)}{\mathbf{f}}. \quad (34)$$

If $N = N_B - 1$, matrix $\mathbf{A}_n$ is a lower triangular matrix. From equation (34), we can find the force vector $\mathbf{f}$ directly:

$$\mathbf{f} = \left(\sum_{n=1}^{N_m} \mathbf{A}_n \right)^{-1} \ddot{\mathbf{v}}. \quad (35)$$

If $N > N_B - 1$ and/or more than one bending moment is measured ($N_L > 1$), the least squares method can be used to find the force vector $\mathbf{f}$

$$\mathbf{f} = \begin{bmatrix} \left(\sum_{n=1}^{N_m} D_{xn}\mathbf{A}_n \right)_1 \\ \left(\sum_{n=1}^{N_m} D_{xn}\mathbf{A}_n \right)_2 \\ \vdots \\ \left(\sum_{n=1}^{N_m} D_{xn}\mathbf{A}_n \right)_{N_L} \end{bmatrix}^+ \begin{Bmatrix} \ddot{\mathbf{v}}_1 \\ \ddot{\mathbf{v}}_2 \\ \vdots \\ \ddot{\mathbf{v}}_{N_L} \end{Bmatrix}. \quad (36)$$

2.4. IDENTIFICATION FROM BENDING MOMENTS AND ACCELERATIONS

If the bending moments and acceleration responses are measured at the same time, both of them can be used together to identify the moving force. The vectors $\mathbf{m}$ in equation (21) and $\ddot{\mathbf{v}}$ in equation (34) should be scaled to have dimensionless units; then the two equations are combined, to give

$$\begin{bmatrix} \mathbf{B}/\|\mathbf{m}\| \\ \mathbf{A}/\|\ddot{\mathbf{v}}\| \end{bmatrix} \mathbf{f} = \begin{Bmatrix} \mathbf{m}/\|\mathbf{m}\| \\ \ddot{\mathbf{v}}/\|\ddot{\mathbf{v}}\| \end{Bmatrix} \quad (37)$$

where $\|\bullet\|$ is the norm of the vector.

2.5. SPECIAL ASPECTS IN IMPLEMENTATION

2.5.1. *Sampling frequency and record length*

The sampling frequency f_s should be high enough so that there is sufficient accuracy in the discrete integration in equations (14) and (26). The f_s/f_a ratio should in general be larger than 5, where f_s is the sampling frequency and f_a is the highest analysis frequency of interest. For the data logging system used in the present study, the hardware poses a limiting f_s/f_a ratio of 2·56, and therefore interpolation of the time history of the measured bending moments and accelerations is required. The number of data N should be equal to or larger than $N_B + 1$.

2.5.2. *Using bending moments or accelerations*

Measurements of the bending moment contain system information mainly in the lower frequency bandwidth, while those of the acceleration contain system information in the higher frequency bandwidth. It should be noted that the static component of the force cannot be identified from acceleration alone. For the general dynamic force identification (e.g., the interaction forces between the bridge and vehicles), it would be more beneficial to use both the bending moment and acceleration measurements.

2.5.3. *Locations at which the responses are measured*

The locations of measurements should be selected carefully because of the presence of modal nodes. The responses of all modes in the analysis frequency bandwidth should be detectable at the measuring point. For example, if there are three modes in the frequency bandwidth of interest, and if the responses at only one location are used, the measurement location should be at 1/4 span. If the responses at two locations are used, the two measurement locations are recommended to be at 1/4 and 1/2 span.

2.5.4. *Modal parameters of the beam*

Modal parameters are required in the moving force identification. The mode shape functions are particularly important for the calculation. In practice, the modal parameters must be obtained from modal testing. If they are obtained through the finite element method or analytical solutions, they should be corrected using measured data. The discrete mode shapes can then be curve-fitted to obtain the mode shape functions. The flexural stiffness EI in equation (14) should be corrected by measured modal frequencies $\tilde{\omega}_n$:

$$EI_n = \tilde{\omega}_n^2 l^4 \rho / n^4 \pi^4, \tag{38}$$

where equation (38) is derived from equation (4).

2.5.5. *Modal truncation*

The number of modes used in the calculation generally depends on the analysis frequency bandwidth. In practice, only the lowest few modes are used, and as a result modal truncation errors will occur. For beam-like structures the modal density is relatively small, and this error will be insignificant. If the measurement locations are carefully selected, the error can be reduced further. For cases of high modal density, the modal acceleration method can be used to reduce the truncation error.

3. SIMULATION AND RESULTS

3.1. SIMULATION PARAMETERS

To check on the correctness and effectiveness of the proposed method, identification of the following forces is simulated:

(a) single moving force,

$$f(t) = 40\,000[1 + 0{\cdot}1 \sin(10\pi t) + 0{\cdot}05 \sin(40\pi t)] \quad \text{N};$$

(b) two moving forces,

$$f_1(t) = 20\,000[1 + 0{\cdot}1 \sin(10\pi t) + 0{\cdot}05 \sin(40\pi t)] \quad \text{N};$$

$$f_2(t) = 20\,000[1 - 0{\cdot}1 \sin(10\pi t) + 0{\cdot}05 \sin(50\pi t)] \quad \text{N},$$

$$l_s = 4 \text{ m}.$$

The parameters of the beam are as follows: $EI = 1{\cdot}274916 \times 10^{11}$ Nm^2, $\rho = 12\,000$ kg/m, $l = 40$ m, $\xi_1 = 0{\cdot}02$, $\xi_2 = 0{\cdot}02$, $\xi_3 = 0{\cdot}04$, $f_1 = 3{\cdot}2$ Hz, $f_2 = 12{\cdot}8$ Hz, $f_3 = 28{\cdot}8$ Hz. The moving speed is 40 m/s. The analysis frequency bandwidth is from 0 Hz to 40 Hz and therefore the first three modes of the beam are included in the calculation. The sampling frequency f_s is 200 Hz and $N_B = 100$. The record length N is 512, and 110 points are used in the identification.

3.2. SINGLE FORCE IDENTIFICATION

Bending moment and/or acceleration responses at 1/2 span and/or 1/4 span are used. Nine combinations of the responses are adopted as follows:

1/2m.	1/2a.	1/2m. and 1/2a.
1/4m.	1/4a.	1/4m. and 1/4a.
1/2m. and 1/4m.	1/2a. and 1/4a.	1/2m. and 1/4a.

where 1/2 and 1/4 represent the location of the span, and m. and a. represent the bending moment and acceleration responses respectively. White noise is added to the calculated responses to simulate the polluted measurements:

$$\mathbf{m} = \mathbf{m}_{calculated} + Ep \times \| \mathbf{m}_{calculated} \| \times \mathbf{N}_{oise}$$

where Ep is a specified error level; $\mathbf{N}_{oise}$ is a standard normal distribution vector (with zero mean value and unit standard deviation). The following results are obtained.

(1) If $Ep = 0$, i.e., where no noises are added to the measured responses, accurate results are obtained. This means that the proposed method and algorithms are correct.

(2) If $Ep = 5\%$, the simulation of the bending moment and acceleration at 1/4 span are shown in Figures 2 and 3. Both the traces of the Power Spectral Density functions (PSD)s and the time histories match closely with the true ones. The PSDs indicate that errors exist in the higher frequency range. This error level is approximately equivalent to 70 dB dynamic range, which is of the same order as those in a measurement system (65 dB). Therefore this error level could represent typical values in practical situations.

(3) For $Ep = 1\%$ and $Ep = 5\%$, the errors in the simulated forces are shown in Table 1. The errors are calculated by the following equation

$$Error = \frac{\| \mathbf{f}_{identified} - \mathbf{f}_{true} \|}{\| \mathbf{f}_{true} \|} \times 100\%.$$

Some of the identified results are shown in Figure 4.

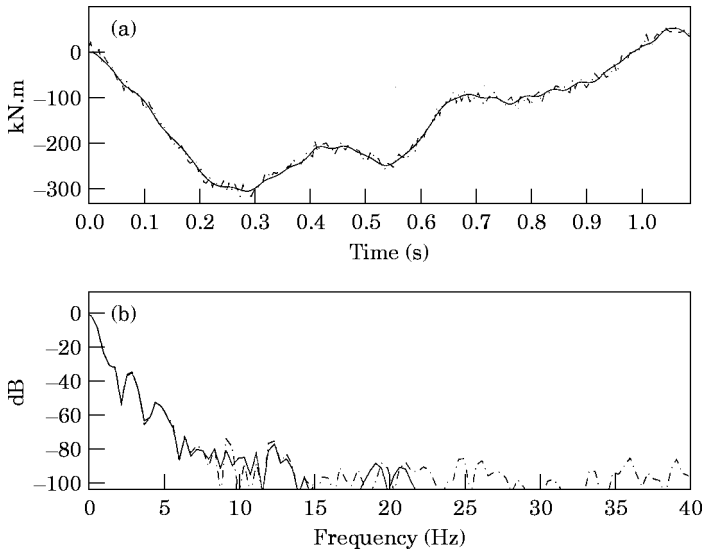

Figure 2. The bending moment at 1/4 span: simulation for single force identification; 40 m/s, 5% error. (a) The 1/4 span bending moment; (b) the PSD of the response. ——, True; –·–·–, simulation.

(4) The results in Table 1 show that the forces identified from bending moments only are inaccurate. That is because the bending moment responses in the high frequency range are very small (refer to Figure 2). It is exactly this phenomenon in the measurements that causes errors in the time domain identification. For the identification of a single moving force, more than one response is required to enhance the identification accuracy.

(5) The results using responses from a single measurement point only are less accurate than those using responses from multi-points, as some of the modal responses may have not been used in the identification.

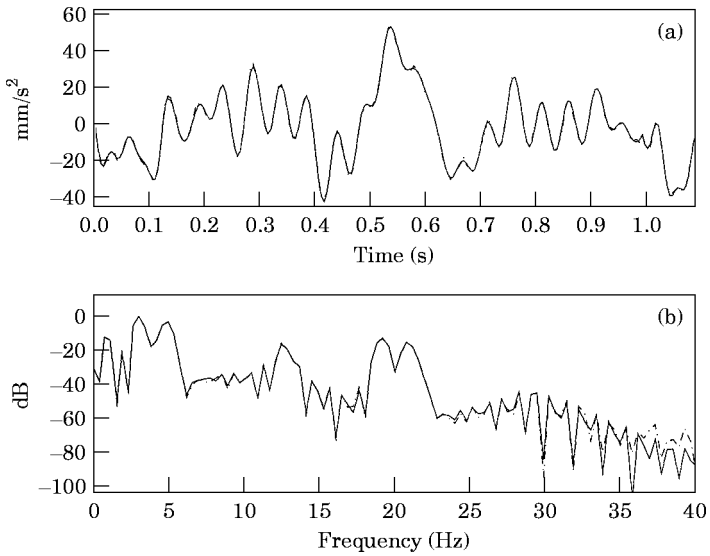

Figure 3. The acceleration at 1/4 span: simulation for single force identification; 40 m/s, 5% error. (a) The 1/4 span acceleration; (b) the PSD of the response. ——, True; –·–·–, simulation.

TABLE 1

Errors on single force identification (in percent)

Location and responses	1% error in response			5% error in response		
	m.	*a.*	*m.* and *a.*	*m.*	*a.*	*m.* and *a.*
1/2	†	16·4	1·32	†	24·9	13·2
1/4	46·4	0·80	0·733	†	3·80	3·57
1/2 and 1/4	24·1	0·24	0·748	†	1·39	3·45

† Error larger than 100%.

(6) The simulation results show that if the bending moment and acceleration are used at the same time, satisfactory results on a single force identification could be achieved for practical cases.

3.3. TWO-FORCES IDENTIFICATION

Bending moment and/or acceleration responses at 1/4, 1/2 and 3/4 spans in 12 combinations described in Table 2 are used to identify the two forces. In a manner similar to single force identification, the following results are obtained.

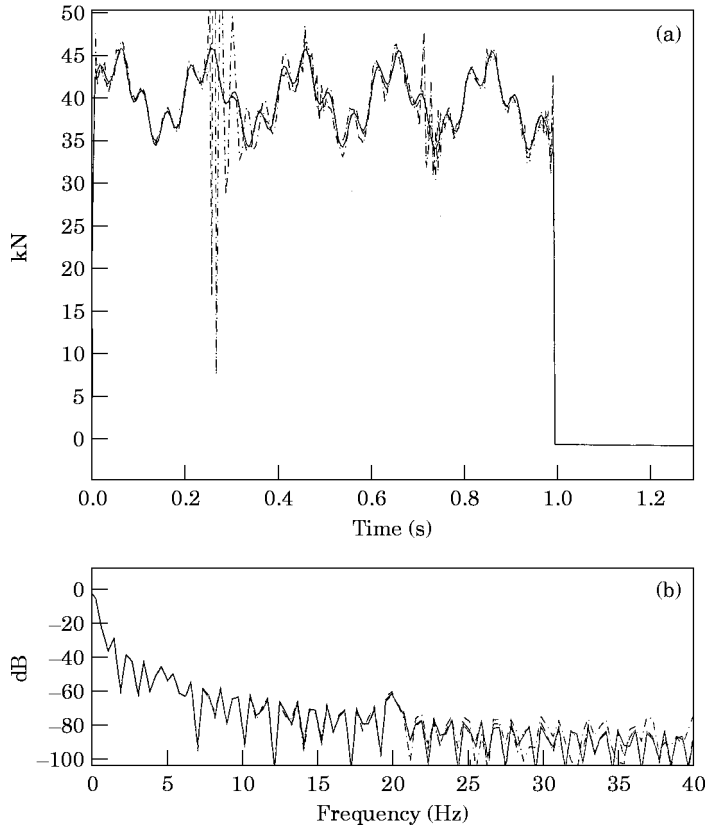

Figure 4. The identified force from simulated single force identification; 40 m/s, 5% error, identified from moments and acceleration. (a) The moving force; (b) the PSD of the force. ——, True force; –·–·–, 1/2*m.* and *a.*; ——, 1/4*m.* and *a.*; · · · ·, 1/2*m.* and 1/4*a.*

TABLE 2

Errors on two-forces identification (*in percent*)

Response combinations, location and response	1% error in response		5% error in response	
	First force	Second Force	First force	Second force
1/2*m*. and 1/4*m*.	421	620	†	†
1/2*m*. and 1/4*m*. and 3/4*m*.	428	397	†	†
1/2*a*. and 1/4*a*.	26·9	12·4	222	78·6
1/2*a*. and 1/4*a*. and 3/4*a*.	3·26	6·34	10·7	10·7
1/2*m*. and 1/2*a*.	266	580	†	†
1/2*m*. and 1/4*m*. and 1/2*a*.	199	360	†	474
1/2*m*. and 1/4*m*. and 1/2*a*. and 1/4*a*.	26·9	13·7	201	49·7
1/4*m*. and 1/4*a*.	813	402	†	†
1/4*m*. and 1/4*a*. and 1/2*a*.	28·2	13·9	206	156
1/2*m*. and 1/4*a*.	162	353	†	†
1/2*m*. and 1/4*a*. and 1/4*m*.	171	224	†	†
1/4*a*. and 1/2*a*. and 1/2*m*.	27·1	13·5	193	46·8

† Error larger than 1000%.

(1) If $Ep = 0$, i.e., when no noises are added to the measured responses, accurate results are obtained. This means that the proposed method and algorithms for two-forces identification are correct.

(2) For $Ep = 1\%$ and $Ep = 5\%$, errors in the identification results are shown in Table 2. Samples of the time histories and PSDs of the identified forces are shown in Figures 5 and 6. The results obtained from using 1/4*a*. and 1/2*a*. vary greatly close to the beam ends and at the nodal points of the third mode of the beam, while those obtained from 1/4*a*., 1/2*a*. and 3/4*a*. give satisfactory results except at both end of the beam. The results are very noise sensitive. The identified forces are close to the true forces only when they are in the middle length of the beam.

(3) Other results not included here show that acceleration measurement gives much better results than bending moment measurements in the identification.

(4) The results also show that accuracy in two-forces identification is lower than in single force identification. One reason is that there is a force component with same amplitude and opposite phase in the two identified forces. This results in large errors in the time domain. Moreover, in Figures 5 and 6 it is shown that there are large errors in the time duration from 0·1 s to 0·3 s and from 0·8 s to 1·0 s. This is due to the low sensitivity of the responses to the forces at the beginning and end of the beam. This results in large errors in the PSDs and time histories of the forces.

4. EXPERIMENTAL RESULTS

4.1. EXPERIMENTAL SET-UP

The experimental set-up is shown diagrammatically in Figure 7. The main beam, 3376 mm long with a 100 mm × 25 mm uniform cross-section, is simply supported. The leading beam is for the acceleration of the model car and the trailing beam is for the slowing down of the car. Some damping material is placed beneath the main beam to improve its damping properties.

A U-shaped aluminum section is glued to the upper surface of the beams as a direction guide for the car. The model car is pulled along the guide by a string wound

around the drive wheel of an electric motor, the rotational speed of which can be adjusted. Seven photoelectric sensors are mounted on the beams to measure and monitor the moving speed of the car. The second sensor is located at the point at which the front wheels of the car just get on the main beam, and the last sensor is located at the point at which the rear set of wheels just get off the main beam. They are used to measure the speed of the model car. The others are located on the beams at a spacing of 0·776 m to check on the uniformity of the speed.

Three strain gauges and four accelerometers are mounted at the bottom of the main beam to measure the responses. One gauge and one accelerometer are mounted at each cross-section, at 1/4, 1/2 and 3/4 span. The fourth accelerometer is mounted at 3/8 span. An eight-channel dynamic testing and analysis system (DTAS) is used for data collection and analysis in the experiment. The first channel is used to monitor the signal of the photoelectric sensors. The second, third and fourth channels are used to measure the signals from the strain gauges. The remaining channels are used to measure the acceleration responses. The sampling frequency is 256 Hz, with a data block size of 2048.

The model car has two axles at a spacing of 0·203 m and it runs on four rubber wheels. The mass of the whole car is 7·1 kg. The modal frequencies and damping ratios obtained from modal testing are shown in Table 3.

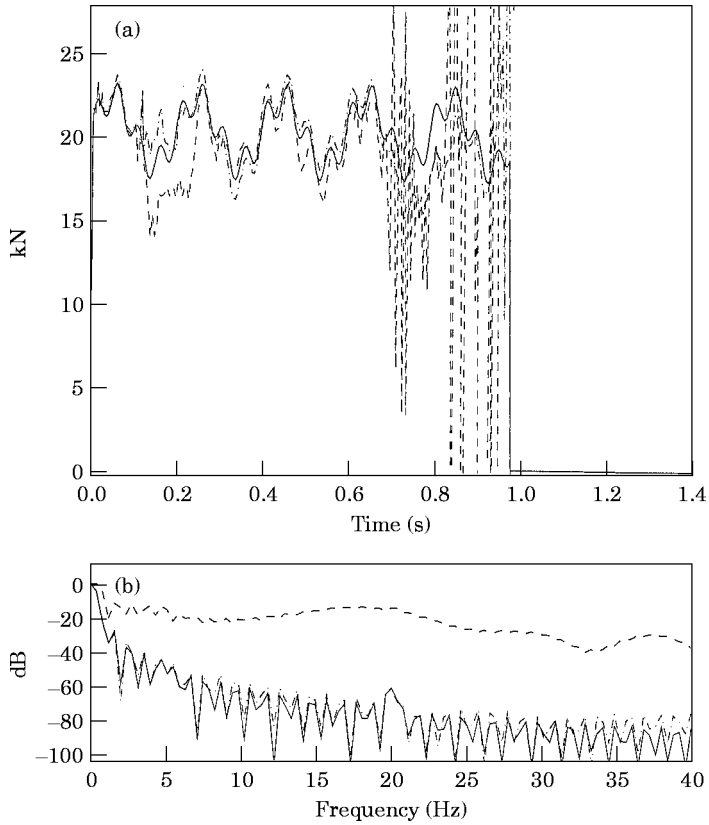

Figure 5. The identified first force from simulated two-forces identification; 40 m/s, 5% error in the responses. (a) The moving force; (b) the PSD of the force. ——, True force; – – –, 1/4a.&1/2a.; –· –· –, 1/4a. and 1/2a. and 3/4a.

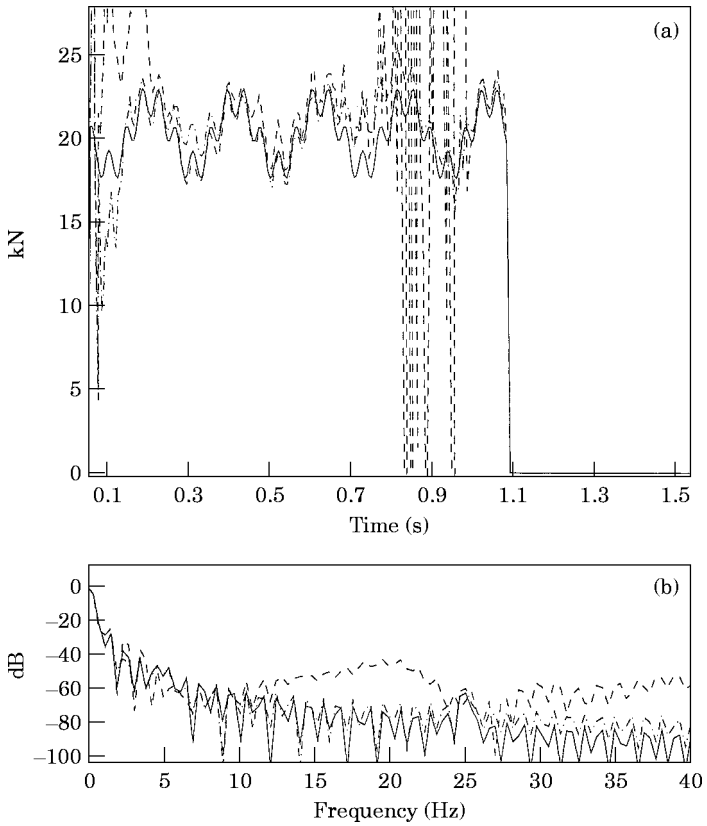

Figure 6. The identified second force from simulated two-forces identification; 40 m/s, 5% error in the responses. (a) The moving force; (b) the PSD of the force. Key as Figure 5.

4.2. EXPERIMENTAL PROCEDURE

(1) A modal test was performed for the model car.

(2) A modal test was performed for the main beam; the modal parameters measured are shown in Table 4. The model shapes were obtained through curve fitting of the measured shapes. The modal masses were obtained and checked by additive masses. The results show that the modal frequencies are different from the calculated results for a simply supported beam and, therefore, the flexural stiffness EI of the beam was corrected using equation (27).

(3) The output of channels 2, 3 and 4 for the strain gauges was adjusted to zero when the main beam was unloaded. This takes care of the fact that the signal from the strain gauges are very small and usually have a zero-shift phenomenon. Removing the zero-shift portion in the output increases the dynamic range of the measurement.

(4) The strain gauges were calibrated by adding masses at the middle of the main beam. The average sensitivities were found to be 2·243, 2·532 and 2·259 mV/N-m, respectively, for the 1/4, 1/2 and 3/4 span gauges. During the calibration, the signal of the strain gauges were found to be not very stable and repeatability was not completely satisfactory. It is noted that this will lead to calibration errors in the identified results.

(5) The car was placed at the left end of the leading beam, and DTAS set in pre-trigger state at channel 1. The power for the motor was turned on, and the car moved on top

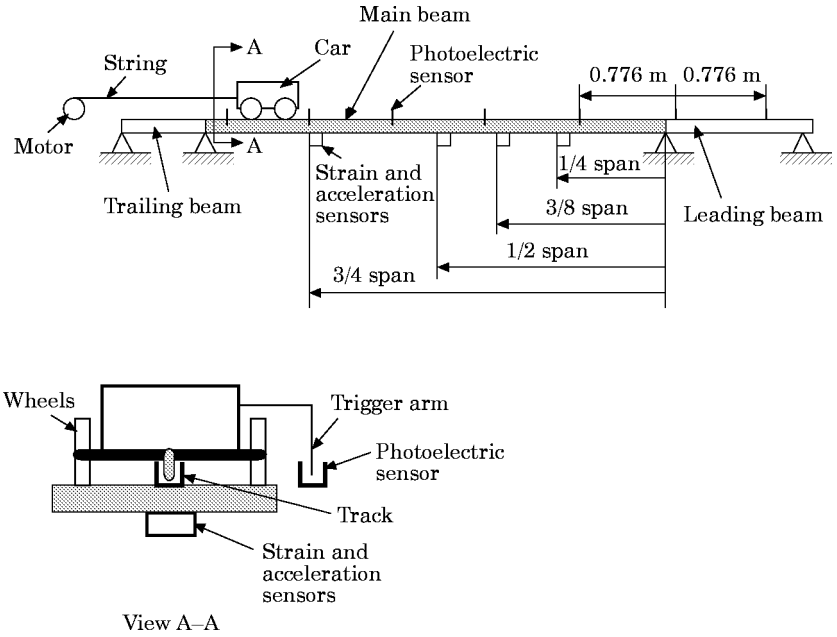

Figure 7. A diagram of the experimental set-up.

of the beams. Eight channels of signal were acquired, samples of which are shown in Figure 8.

(6) The speed was calculated and the uniformity of the speed checked.

(7) If the speed was stable, steps (2)–(4) were repeated to check whether or not the properties of the structure and measurement system had changed. If no significant change was found, the recorded data was accepted.

(8) The zero-shift in the measured signals was removed, and the signals were calibrated using measured channel sensitivities. The point in the signals at which the front wheel of the car just got on the main beam was identified.

TABLE 3

The modal parameters of the model car

Mode	Frequencies (Hz)	Damping ratios (%)	Mode type
1	27·5	10·5	Bounce
2	42·9	11·7	Pitch
3	69·4	10·8	Roll

TABLE 4

The modal parameters of the main beam

Mode	Frequencies (Hz)	Damping (%)	Mode shapes	Modal masses (kg)	Corrected EI (kN-m^2)
1	6·612	2·71	$\sin(\pi x/3{\cdot}776)$	40·13	63·4
2	18·51	0·653	$\sin(2\pi x/3{\cdot}776)$	38·58	31·1
3	39·45	0·199	$\sin(3\pi x/3{\cdot}776)$	38·65	28·6

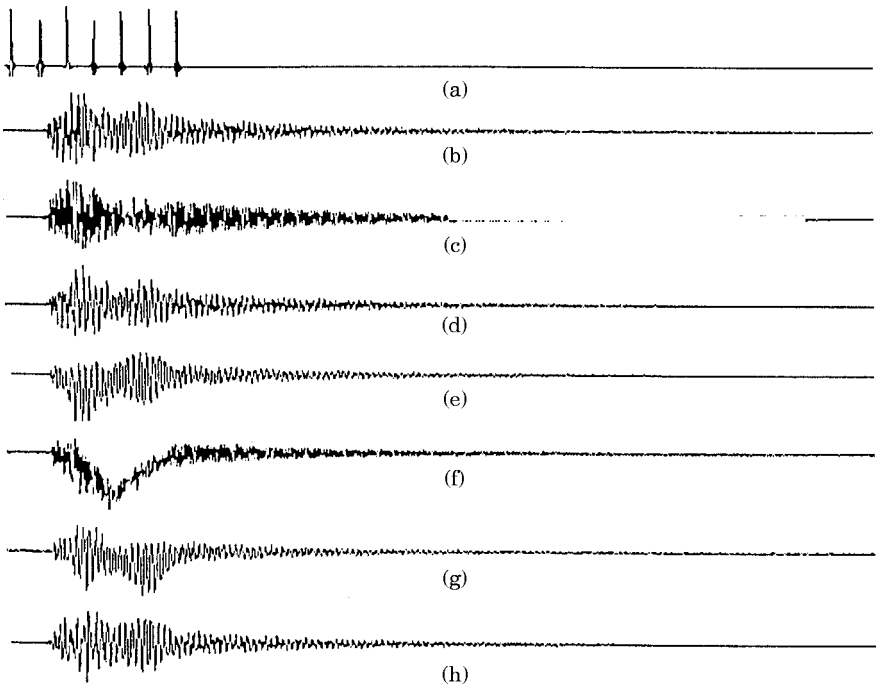

Figure 8. The recorded time histories from sensors in the experiment. (a) Channel 1, photoelectric sensor signal; (b) channel 2, acceleration at 1/4 span; (c) channel 3, acceleration at 1/2 span; (d) channel 4, acceleration at 3/4 span; (e) channel 5, bending moment at 1/4 span; (f) channel 6, bending moment at 1/2 span; (g) channel 7, bending moment at 3/4 span; (h) acceleration at 3/8 span.

(9) Interpolation between two measured points in the time histories of the responses was carried out, if necessary, to ensure a sampling frequency at least five times the highest analysis frequency of interest.

(10) The interaction forces were identified as a single moving force using the bending moment and acceleration responses at 1/4 and 1/2 span, and the identified results were indirectly checked by comparing the measured bending moment and acceleration at 3/4 span with the responses calculated from the identified force.

(11) The interaction forces were identified as two moving forces using the bending moment and acceleration responses at 1/4, 1/2 and 3/4 span, and the identified results were

TABLE 5

The correlation coefficients between measured and calculated responses: single force identification

Combinations of the responses	Comparing bending moment at 3/4 span	Comparing acceleration at 3/4 span
1/2*m*.	0·140	0·076
1/4*m*.	0·845	0·416
1/2*m*. and 1/4*m*.	0·942	0·584
1/2*a*.	0·674	0·252
1/4*a*.	0·793	0·565
1/2*a*. and 1/4*a*.	0·792	0·565
1/2*m*. and 1/2*a*.	0·775	0·814
1/4*m*. and 1/4*a*.	0·810	0·755
1/2*m*. and 1/4*a*.	0·818	0·844

indirectly checked by comparing the measured acceleration at 3/8 span with the responses calculated from the identified forces. Due to the limitations of the available measurement channels, only the acceleration at 3/8 span was used for checking.

4.3. SINGLE FORCE IDENTIFICATION

Nine combinations of the measured responses are used to identify the force. The responses of the main beam at 3/4 span are calculated using the identified force, and they are compared with the measured responses. Correlation coefficients between the calculated and measured responses are calculated to evaluate the accuracy of the identified force. Clearly, a larger coefficient means that the identified force is more accurate than that with a smaller coefficient, but the larger coefficient does not mean the identified force is accurate enough, because this indirect method of checking of the identified results is not fully sufficient. The coefficients are shown in Table 5, and some of the identified results are shown in Figures 9–11.

It is not possible to identify the static component of the forces using only acceleration measurements, and the static forces are added to the identified forces in the figures for convenience of comparison.

The results in Table 5 show that the combined use of bending moment at 1/2 span and acceleration at 1/4 span is most suitable for single moving force identification. In Figures 10 and 11 it is shown that the PSDs of the responses match very closely, although

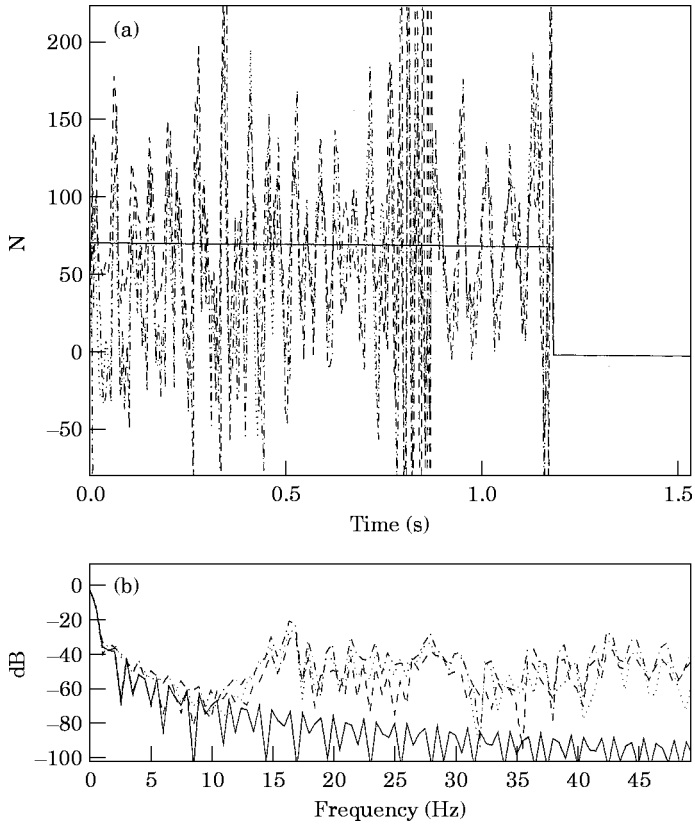

Figure 9. The identified force from experimental single force identification; 3·102 m/s, identified from bending moments. (a) The moving force; (b) the PSD of the force. ——, Static; –· –· –, 1/2 and 1/4m.; ——, 1/2 and 1/4a.; · · · ·, 1/2m. and 1/4a.

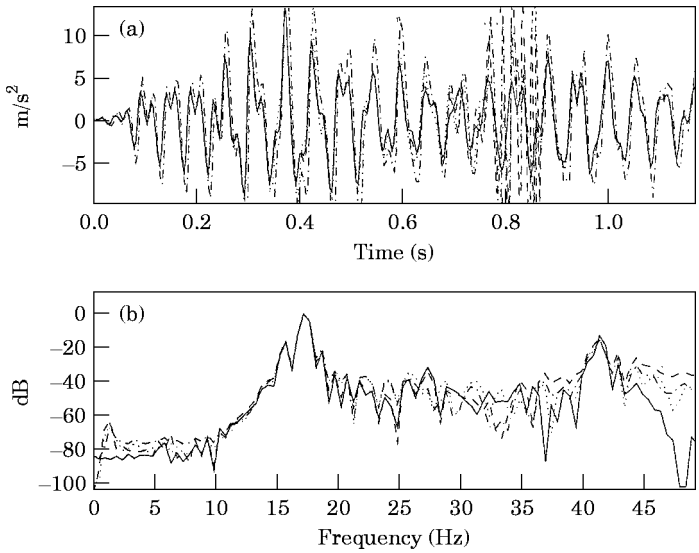

Figure 10. The measured and calculated acceleration at 3/4 span: experimental single force identification; 3·102 m/s. (a) The measured and calculated accelerations at 3/4 span; (b) the PSD of the response. ——, Measured. Identified: –·–·–, 1/2 and 1/4*m*.; – – –, 1/2 and 1/4*a*.; · · · ·, 1/2*m*. and 1/4*a*.

the time histories are not very close to each other. It is suspected that calibration errors lead to these differences in the time histories. The PSDs of the identified forces from bending moments in Figure 9 match loosely, but the identified forces in the time domain at several time intervals are below zero, which could not be explained using the experimental observations.

4.4. TWO MOVING FORCES IDENTIFICATION

Twelve combinations of the measured responses are used to identify the two forces. The acceleration of the main beam at 3/8 span is calculated using the identified forces, and it

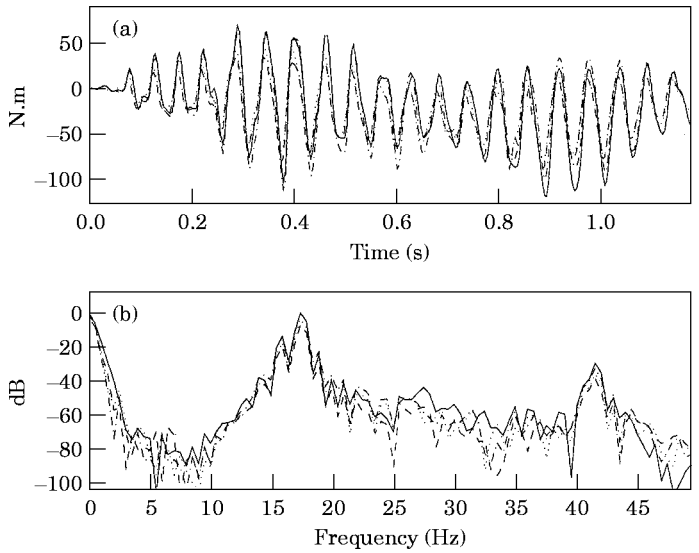

Figure 11. The measured and calculated bending moments at 3/4 span: experimental single force identification; 3·102 m/s. (a) The measured and calculated bending moments at 3/4 span; (b) the PSD of the response. Key as Figure 10.

TABLE 6

The correlation coefficients between measured and calculated responses: two-forces identification

Response combinations, location and response	Correlation coefficient
1/2*m*. and 1/4*m*.	0·640
1/2*m*. and 1/4*m*. and 3/4*m*.	0·708
1/2*a*. and 1/4*a*.	0·933
1/2*a*. and 1/4*a*. and 3/4*a*.	0·994
1/2*m*. and 1/2*a*.	0·989
1/2*m*. and 1/4*m*. and 1/2*a*.	0·856
1/2*m*. and 1/4*m*. and 1/2*a*. and 1/4*a*.	0·883
1/4*m*. and 1/4*a*.	0·865
1/4*m*. and 1/4*a*. and 1/2*a*.	0·870
1/2*m*. and 1/4*a*.	0·874
1/2*m*. and 1/4*a*. and 1/4*m*.	0·856
1/4*a*. and 1/2*a* and 1/2*m*.	0·863

is compared with the measured response. Correlation coefficients are calculated between the calculated and measured responses, and they are shown in Tables 6. Some of the identified results are shown in Figures 12–14.

The results from Table 6 show that the acceleration response alone or combined bending moment and acceleration responses are suitable for the two-forces identification. Comparison of the correlation coefficients of the accelerations in Table 5 and 6, and comparison with Figures 11 and 14, show that results from the identification of two moving forces are more accurate than those from the identification of a single force.

Large discrepancies in the identified results around 0·065 s and 1·025 s are shown in Figures 12 and 13. These two moments correspond to the entry of the second axle and the exit of the first axle to the bridge, where the forcing system switches from a single force excitation to a two-forces excitation and *vice versa*. The large discrepancy after 1 s

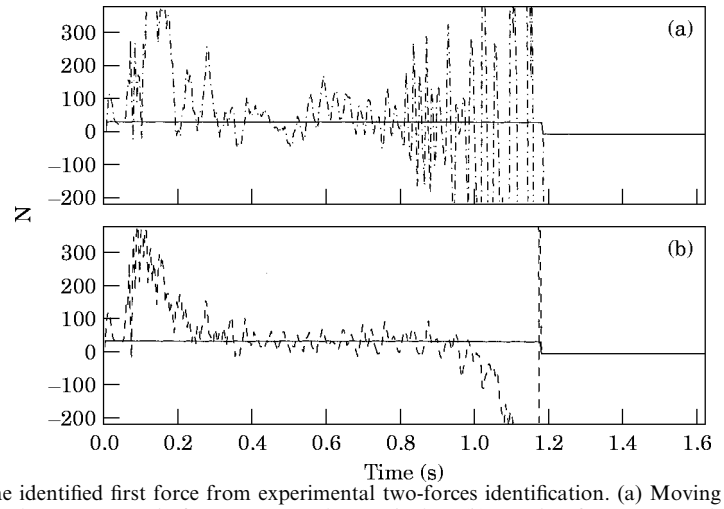

Figure 12. The identified first force from experimental two-forces identification. (a) Moving force, 3·102 m/s using 1/4*a*. and 1/2*a*.: ——, static force; –·–·–, 1/4*a*. and 1/2*a*. (b) Moving force, 3·102 m/s using 1/4*a*. and 1/2*a*. and 3/4*a*.: ——, static force; ——, 1/4*a*. and 1/2*a*. and 3/4*a*.

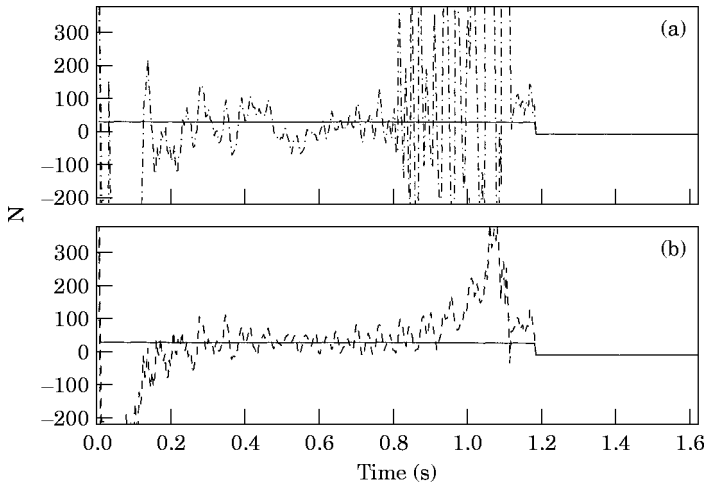

Figure 13. The identified second force from experimental two-forces identification. Key as Figure 12.

corresponds to the incorrect identification by the proposed method of non-existent forces on the bridge deck, due to free oscillation of the structure.

There is also a large local discrepancy between the identified results and the true force using 1/2 and 1/4 accelerations at around 0·87 s in Figures 12–14. This occurs as the vehicle is located on the nodal point of the third mode shape of the beam, and the noise from the third modal frequency bandwidth would dramatically affect the identified result. Similar phenomena in the simulation results are found in Figures 4–6. The identified results using 1/4, 1/2 and 3/4 accelerations are close to the true static force within the time range of 0·3–0·9 s. This strongly suggests using responses from at least three locations for the identification, to reduce these local discrepancies, and disregarding the good correlation shown in Table 6 for cases using responses from two locations.

By comparing Figures 12 and 13, we find that there is a component with the same amplitude and opposite phase in the two identified forces. This is the component due to

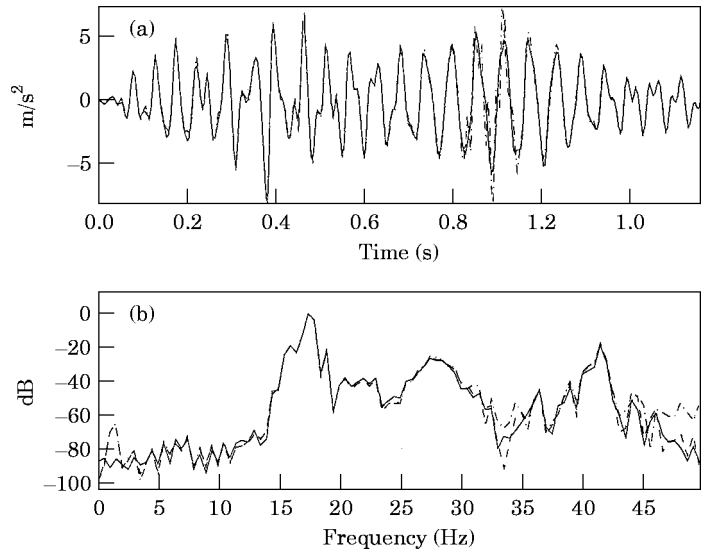

Figure 14. The measured and calculated accelerations at 3/8 span: experimental two-forces identification; 3·102 m/s. (a) Measured and calculated accelerations at 3/8 span; (b) the PSD of the response. ——, Measured; –·–·–, 1/4*a*. and 1/2*a*.; ——, 1/4*a*. and 1/2*a*. and 3/4*a*.

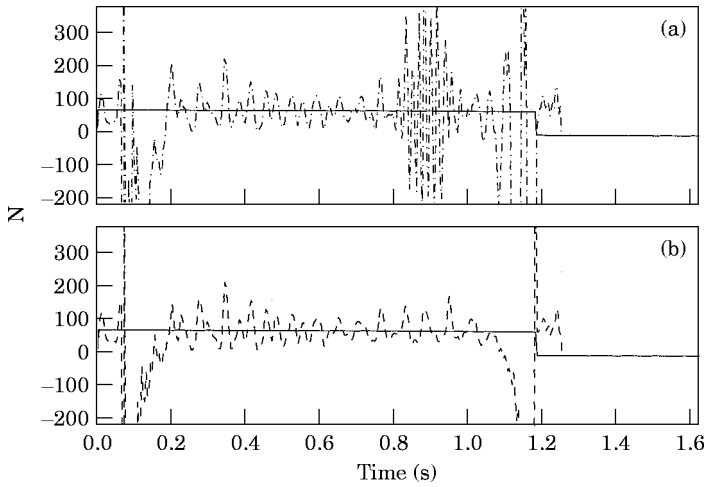

Figure 15. The identified resultant force from experimental two-forces identification. (a) Moving force, 3·102 m/s using 1/4a. and 1/2a.: ——, static force; –·–·–, 1/4a. and 1/2a. (b) Moving force, 3·102 m/s using 1/4a. and 1/2a. and 3/4a.: ——, static force; ——, 1/4a. and 1/2a. and 3/4a.

the pitching motion of the model car. The two identified forces are added to obtain a resultant force, as shown in Figure 15. This resultant force matches the true force very closely. This resulting force is a good estimate of the total dead weight force of the vehicle.

5. DISCUSSION

(1) A vehicle with only a few degrees of freedom has been studied, and it serves to show the important trends and considerations which are applicable to actual vehicles crossing a bridge deck. The vehicle and suspension characteristics (mass and stiffness) are not important in the identification of the interaction forces.

(2) The plots shown for single force and two-forces identification show accurate estimates of the mass of the vehicle, and this method can be used for the WIM (weight-in-motion) of passing vehicles with no constraints on the type of vehicle or its suspension characteristics.

(3) This method is beneficial to the identification of vehicles with only a limited number of axles, since each additional moving force adds another set of equations which must be solved. For the case of many vehicles or multi-axle vehicles, a much greater computational cost will be involved.

(4) It is noted that the use of the finite element method combined with modal analysis in solving this problem gives approximate solutions, especially in the higher frequency range, while the proposed method gives a more reliable estimate, especially when the contributions of higher modes have been checked to be significant for the overall responses of the structure.

6. CONCLUSIONS

The theoretical studies, computation simulations and laboratory experiments suggest the following conclusions.

(1) It is possible to use measured responses to identify moving forces in the time domain.

(2) The agreement between the calculated and measured dynamic responses is, for the most part, quite acceptable. Acceptable results can be obtained using either measured accelerations or a combination of accelerations and bending moments.

(3) It is believed that difficulties may arise in using bending moment measurements to predict the time varying moving forces because of the limitations of the dynamic range in the measurements. Errors in the higher analysis frequency range will lead to large errors in the identified results.

(4) Satisfactory results in terms of computational cost and accuracy could be obtained for single force identification with the proposed method. However, the identification of more than one force needs a longer computational time. Further study is required to increase the accuracy and to reduce the computational costs.

(5) The correlation of the reconstructed and measured responses is a robust scoring function for evaluating the identified results.

ACKNOWLEDGMENT

This study was carried out with the sponsorship of the Research Grants Council of Hong Kong.

REFERENCES

1. D. Williams and R. P. N. Jones 1948 *Aeronautic Research Council*, *TR* # 2221. Dynamic loads in aeroplanes under given impulsive loads with particular reference to landing and gust loads on a large flying boat.
2. J. K. Schueller and T. M. P. Wall 1991 *Experimental Mechanics* **31**, 118–121. Impact of fruit on flexible beams to sense modulus of elasticity.
3. K. K. Stevens 1987 *Proceedings of SEM Spring Conference on Experimental Mechanics*, 838–844. Force identification problems: an overview.
4. J. C. Briggs and M. K. Tse 1992 *International Journal of Impact Engineering* **12**, 361–372. Impact force identification using extracted modal parameters and pattern matching.
5. J. F. Doyle 1994 *Experimental Mechanics* **34**, 37–44. A genetic algorithm for determining the location of structural impacts.
6. J. M. Tunna 1988 *Ninth International Wheelset Congress Paper* 6–2. Wheel/rail forces due to wheel irregularities.
7. J. C. O. Nielsen and T. J. S. Abrahamsson 1992 *International Journal of Numerical Methods Engineering* **33**, 1843–1859. Coupling of physical and modal components for analysis of moving non-linear dynamic systems on general beam structures.
8. C. O'Connor and T. H. T. Chan 1988 *Journal of Structural Engineering* **114**, 1703–1723. Dynamic wheel loads from bridge strains.

APPENDIX: NOTATION

c	speed of vehicle	p_n	modal force of nth mode
C	viscous damping of beam	q_n	nth modal amplitude
E	Young's modulus of material	v	deflection of beam
f_a	highest analysis frequency of interest	$\delta(t)$	Dirac delta function
f_s	sampling rate	ρ	mass per unit length of beam
$f(t)$	time varying concentrated force	ω_n	nth modal frequency
I	second moment of inertia	ω_n'	damped nth modal frequency
l	length of beam	$\tilde{\omega}_n$	measured nth modal frequency
l_s	axle distance	ξ_n	damping ratio of nth mode
m	bending moment	Φ_n	mode shape function of nth mode
M_n	modal mass of nth mode	$\mathbf{f}$	force vector
n	mode number	$\mathbf{m}$	bending moment vector
N	number of discrete data point	$\ddot{\mathbf{v}}$	acceleration vector
N_B	number of discrete data point when vehicle is on beam	$\|\bullet\|$	norm of vector $\lfloor\bullet\rfloor$